Representing Wave Energy Converters in the SWAN model with varying transmission coefficients across frequencies

Matías Alday G., Vaibhav Raghavan, and George Lavidas

Abstract—**Understanding the effects of arrays of Wave Energy Converters (WEC) on the wave fields is still an ongoing effort. Many publications have proposed different approaches to incorporate WEC farms in wave models to assess sea state changes in the near and far field. In the present study, a practical iterative method is proposed to incorporate the spectral response of a WEC obtained from HAMS-MREL in the SWAN spectral wave model. This allows to change the transmission properties of the WEC, represented in the model as an obstacle, at each time step. Since the response of a WEC simulated in a Boundary Element Method (BEM) model is defined in the frequency domain, it is possible to relate the absorbed power, at each discrete frequency, to the transmission coefficient applied at each frequency used to discretize the wave spectrum in SWAN. In this case, the method is applied to a single point-absorber type device since its response is independent of the waves' directions. Further adjustments of the method should be done comparing the spectrum obtained downwave of the WEC in SWAN, with the spectrum reconstructed using the regular wave fields information from HAMS-MREL.**

Index Terms—**HAMS-MREL, SWAN, WEC, Wave spetrum, ...**

I. Introduction

THE development of types and technology of Wave Energy Converters (WECs) keeps progressing, pushing towards commercialization as the global demand for alternative sources of energy increases. In this sense, the spatial projection of WEC arrays is a necessary step to optimize layouts, and quantify operational interactions, effects production and economic feasibility (e.g.; [1]–[3]). At the same time, predicting the effects of WECs on the wave field can be of great importance when large arrays are projected, especially for environmental impact studies. Depending on the WEC arrays layout, number of devices and depths of deployment, it is expected to have changes in the wave field characteristics in the near and far fields. In the latter case, these changes can possibly affect coastal processes in the nearshore [4]–[7].

Many studies based on numerical modelling, have progressively improved our understanding of the extent of WECs' effects on the sea states characteristics. Employing different approaches to incorporate WEC devices in wave models, these publications have also helped to clarify the benefits and shortcomings of the different proposed methods [8]–[11]. In the preset paper, we present a practical method to incorporate the response of a WEC obtained from the HAMS-MREL [12] Boundary Element Model (BEM), in the SWAN spectral wave model [13], [14]. The aim of this method is to emulate the WEC's operation with optimized PTO values (linked to the incoming sea states), in the wave model. This is done relating the absorbed power per frequency obtained in HAMS-MREL and available wave power, at a specific time step, to a frequency dependent transmission coefficient $K_t(f)$ in SWAN. In this case, a point-absorber device is represented as a closed polygon which acts as partial sink element, with changing characteristics in time. It should be noticed that, at this stage, the radiated wave components generated from the WEC's operation are not considered in SWAN.

Both, HAMS-MREL and SWAN, operate in the spectral (or frequencies) domain. This implies that simulations require low computational resources and running time compared to time domain WEC models or phase solving wave models. Therefore, the proposed approach can help to improve the accuracy of results for long term (i.e. > 10 years) assessments of WEC farms' effects on the wave field characteristics.

In the present study, the method description is included in Section II, with the obtained results in Section III, followed by a brief discussion in Section IV.

II. Materials and method

A. HAMS-MREL model

The hydrodynamic model developed with HAMS-MREL is used to estimate the power per frequency absorbed by the WEC. Using time series of variance spectra, the power absorbed per frequency is used to construct power spectra time series, which is later utilized to obtain the transmission coefficient in SWAN (see Section II-C).

The geometry and mass properties of the point absorber devices are inspired by the Corpower C4 device [15]. The dimensions of the device are given in Table I. A weakly non-linear frequency domain model, only considering heave motion, was used for estimating the motion of the device per frequency, considering

M. A., V. R. and G. L. are part of the Marine Renewable Energies Lab (MREL) from the Offshore Engineering Section of the Delft University of Technology (TU Delft), Stevinweg 1, 2628 CN Delft, The Netherlands (e-mail: m.f.aldaygonzalez@tudelft.nl, v.raghavan@tudelft.nl, g.lavidas@tudelft.nl).

Digital Object Identifier:
https://doi.org/10.36688/ewtec-2025-866

viscous losses. The viscous losses are calculated using the spectral domain method [16], [17], which are well suited for irregular sea states.

Passive control is adapted for the WEC, which utilizes an optimized PTO coefficient based on the work of Hals et.al [18]. The motion for the i^{th} frequency ω_i is estimated with the following expression:

$$[-\omega_i^2(m_d + m_{a,i}(\omega_i)) + i\omega_i(b_{a,i}(\omega_i) + b_{PTO} + b_v) + c_h]s = f_{e,i}(\omega_i) \quad (1)$$

where the first 2 terms are the mass of the device m_d and the added mass heaving hydrodynamic coefficient $m_{a,i}$. Then, $b_{a,i}$ is the radiation damping heaving hydrodynamic coefficient, b_{PTO} is the PTO coefficient for the device, b_v is the linearized viscous damping coefficient. Finally, c_h is the hydro-static stiffness coefficient in heaving, $f_{e,i}$ is the heave exciting force, and s is the displacement amplitude of the device also referred to as the body excursion. When the amplitude of the incident wave is 1 m, then s represents the RAO (Response amplitude Operator) in heave motion for the device.

The frequency dependent hydrodynamic coefficients and exciting forces are obtained from the solver HAMS-MREL. The mesh employed for running the simulations in HAMS-MREL is shown in Fig. 1.

In order to estimate the optimal passive PTO coefficient for a given irregular sea state, the transferred method [19] is used, wherein an equivalent regular sea state is obtained from the irregular sea state based on energy equivalence. For an irregular sea state represented by H_s and T_p, the equivalent regular sea state can be estimated with $H_s/\sqrt{2}$ and T_e, where T_e is the energy period and can be estimated as $0.9T_p$ [20]. The hydrodynamic coefficients and exciting forces in heaving are estimated for this regular sea state and then used to estimate the optimal passive damping coefficient b_{PTO}.

TABLE I
PROPERTIES OF THE POINT ABSORBER DEVICE

Property	Value	Unit
Diameter	9	m
Height	18	m
Weight	70	T
Buoy Draft	6	m
Undamped Natural period (heave)	3	s

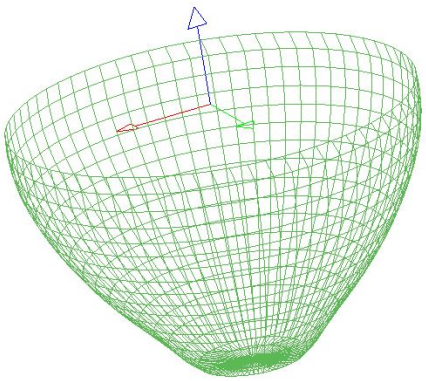

Fig. 1. Mesh of Point absorber modelled using HAMS-MREL

Estimating the optimal passive damping coefficient b_{PTO} and the response in irregular sea states utilizing spectral domain calculation for the viscous damping requires an iterative procedure, that has been utilized by the authors in Alday et al. [21].

Once the responses per frequency are estimated, the power per frequency can be estimated as

$$P_{abs}(\omega_i) = \frac{1}{2} b_{PTO} \omega_i^2 |s_i|^2 \cdot a(\omega_i)^2 \quad (2)$$

where

$$a(\omega_i) = \sqrt{2E(\omega_i)\Delta\omega_i} \quad (3)$$

where $E(\omega_i)$ is the variance spectrum for any given time step, and $\omega_i = 2\pi f_i$.

B. SWAN model setup

SWAN (Simulating WAves Nearshore) is a spectral wave model specially developed for applications in coastal zones. It solves the Eulerian formulation of the (discrete) spectral balance of wave action (4). The model can be driven by winds and boundary conditions and it accounts for processes such as: wind-wave generation, nonlinear wave-wave interactions, white-capping, wave-current interactions, depth-induced refraction, wave dissipation due to bottom friction and depth induced breaking (to name a few).

$$\frac{\partial N}{\partial t} + \frac{\partial}{\partial x} C_x N + \frac{\partial}{\partial y} C_y N + \frac{\partial}{\partial \sigma} C_\sigma N + \frac{\partial}{\partial \theta} C_\theta N = \frac{S}{\sigma} \quad (4)$$

The evolution of the wave spectrum is described by (4), where N is the wave action density. The terms on the left-hand side of the equation are: First, local rate of change of action density in time; Second and third terms are the propagation of wave action in the geographical space with celerity C_x and C_y; The fourth term is relative frequency (σ) due to variation in depth and currents with propagation velocity C_σ; The fifth term is the depth-induced and current-induced refraction with propagation velocity C_θ in the directional space θ. All the propagation speed terms are taken from the linear wave theory [22], [23]. The S/σ term on the right-hand side of (4) corresponds to all the source terms included in the model as physical parameterizations, such as the nonlinear wave-wave quadruplets and triads [24], [25]. For further details on the SWAN model, please refer to the SWAN user and scientific manuals [26], [27].

In the present study we consider a model domain of 505 m by 405 m, along the x and y axis respectively, with a spatial resolution (Δx and Δy) of 5 m. The wave spectrum is discretized in 180 directions (2° resolution) and 32 frequencies from 0.034 to 0.65 Hz. Frequencies

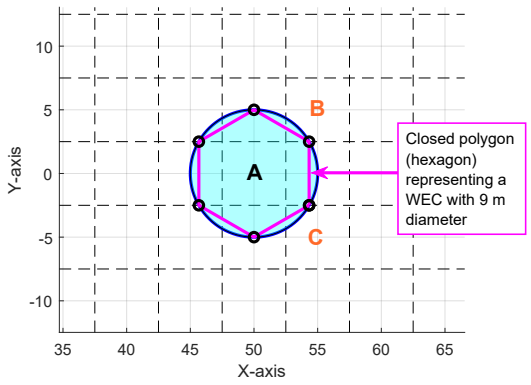

Fig. 2. WEC representation in SWAN. Dashed Gray lines show the computational grid cells, black circles are the points defining the close hexagon. A (50,0), B (55,5) and C (55,-5) are control locations where wave spectra is requested.

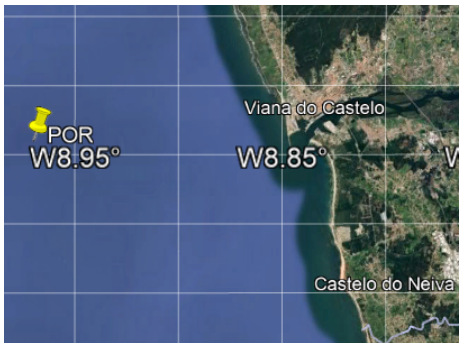

Fig. 3. Location at which directional spectra is taken from the ECHOWAVE hindcast and used as boundary conditions in SWAN. Specific POR coordinates are : Lon: $41.68°$, Lat: $-8.97°$

have a logarithmic distribution with a 1.1 factor between each one of them (see recommendations in [26]). The point-absorber WEC described in Section II-A is included in the wave model as a closed hexagon using the subgrid obstacle parameterization [27] (see Fig. 2). This shape was adopted following recommendations from de Leon et al. [28]. The WEC center is located at $x = 50$, $y = 0$. A frequency dependent transmission coefficient $K_t(f)$ is applied to the "obstacle" representing the point-absorber. As explained in Section II-C, the transmission values are updated at each time step.

The model is forced only with spectral boundary conditions taken from the ECHOWAVE hindcast [29]. For this test case, the (hourly) spectra data is taken from the POR location $\sim$ 10 km offshore the coast of Viana do Castelo, Portugal (Fig. 3). The boundary conditions are applied along the West, South and North sides of the computational grid. Additionally, a constant uniform depth of 70 m is considered for the complete modeled domain, matching the depth from where the boundary conditions are taken.

C. Estimation of transmission coefficients per frequency

The response of the WEC varies in time, through optimization of the PTO, to maximize power harvesting under different incoming sea states characteristics. This implies that not only the bulk absorbed power will change, but also its values per frequency. If the presence of the WEC is consider as a "partial sink" of spectral energy in the wave model, then it is possible to estimate its effect based on the computed absorbed power (per frequency) and the available wave resource. Using the information from the wave (omnidirectional) spectrum, the wave power density at each discrete frequency $P_{\text{wave}}(f_i)$ is computed as follows:

$$P_{\text{wave}}(f_i) = \frac{\rho g}{16} C_g(f_i) \left(2a(fi)\right)^2 \tag{5}$$

where f_i corresponds to a discrete frequency. $a(f_i)$ is the amplitude of a regular wave, with frequency f_i, obtained from the spectral density level $E(f_i)$:

$$a(f_i) = \sqrt{2E(f_i)\Delta f_i} \tag{6}$$

The varying "sink effect" of the WEC is then included with the frequency dependent transmission coefficient $K_t(f_i)$. The aim of $K_t(f_i)$ is to allow the down-wave propagation of energy that has not been used by the point-absorber. At each time step, $K_t(f_i)$ is computed with the following expression:

$$K_t(f_i) = 1 - \left(\frac{P_{\text{abs}}(f_i)}{\phi_{\text{wec}} P_{\text{wave}}(f_i)} \right) \tag{7}$$

where ϕ_{wec} is the WEC's diameter.

D. Modelling pipeline

The following steps are considered to include the WEC's operation characteristics in SWAN. Additionally, a diagram of the modelling pipeline is presented in Fig. 4 for further details.

- Hourly time series of estimated absorbed power using HAMS-MREL with "realistic" spectral data from hindcast.
- Time series of $K_t(f_i)$ is generated with results from hourly $P_{\text{abs}}(f_i)$ and spectral data.
- A "pre-run" is done in SWAN without including the WEC in the domain , and with spectral condition from the first time step. This is done to create an initial hot file used in the first run including the point-absorber.
- N number of stationary runs including the WEC are done. Each run corresponds to a time step from the time series of spectral data. Boundary conditions and $K_t(f_i)$ are updated for each run. At the end of every stationary run a hot file is created and then used as the starting wave field for the follow up SWAN run. This allows to reduce the computing time and improves stability of the wave model.

E. Comparison analysis

To evaluate the changes on the wave field, introduced by the WEC operation in SWAN, a comparison is done with simulations using a simpler approach. For the tests presented here, we compare with runs that consider a fixed K_t value for every time step (as done for example in Rute Bento el al. [5] or in Carballo & Iglesias [7]). In this case K_t (8) defines the ratio between the incident significant wave height (H_{si}) and

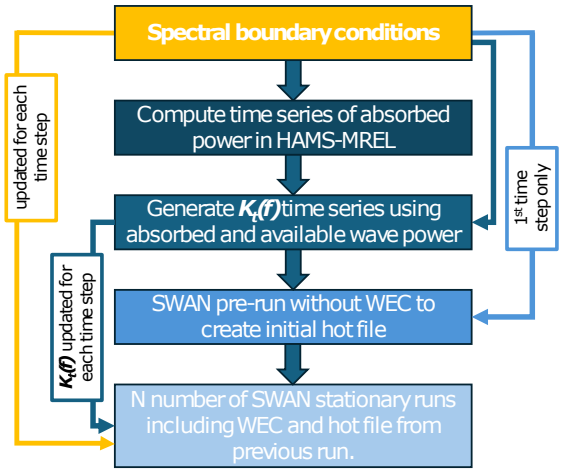

Fig. 4. Modelling flow chart describing the proposed method to include WECs in SWAN.

the transmitted one (H_{st}) intermediately on the downwave side of the WEC.

$$K_t = H_{st}/H_{si} \tag{8}$$

All comparisons are done for 1-month simulations (January 2021), with 1-hourly output data. Changes on the wave field characteristics are assessed in terms of the 1D (omnidirectional) spectrum and wave parameters: significant wave height H_s, peak period T_p and the mean wave period $T_{\mathrm{m}-10}$. To quantify the differences between modelling approaches, the following expressions are used: Mean Differences (9), Normalized Mean Differences (10), and the Normalized Root Mean Squared Differences (11).

$$\mathrm{MD}(X) = \frac{1}{N}\sum(X_a - X_b) \tag{9}$$

$$\mathrm{NMD}(X) = 100\frac{\sum(X_a - X_b)}{\sum X_b} \tag{10}$$

$$\mathrm{NRMSD}(X) = 100\sqrt{\frac{\sum(X_\mathrm{a} - X_\mathrm{b})^2}{\sum X_\mathrm{b}^2}} \tag{11}$$

In equations (9) to (11) X is the analyzed quantity (H_s for example), and a and b denote the modelling approach. In all tests, comparisons are made with respect to results obtained employing the modelling method proposed in this study. For simulations that use a fixed transmission coefficient, $K_t = 0.1$ is employed (as adopted in Wells at al. [30]). NMD and NRMSD are expressed in percentage.

III. Results

A. Differences on wave parameters

As mentioned in Section II-E, we evaluate the changes of the H_s, T_p and $T_{\mathrm{m}-10}$ fields, related to the use of different modelling approaches to represent the effect of the point-absorber. The MD, NMD and NRMSD results are presented in Fig. 5.

In general the use of a fixed $K_t = 0.1$, based on (8), overestimates the WECs operation effects on the wave field. In Fig. 5.a we observe that mean changes of H_s are more significant within the first 30 m away from the WEC position with MD levels close to -0.13 m (NMD of -4.5%). At 50 m away from the device (along the mean wave direction), the MD are close to -0.05 m only (NMD $= -2.2\%$). The NRMSD of H_s shows that the WEC representation approach effects extends a bit further along the mean downwave direction. About 70 m away from the WEC the NRMSD can be close to 3%. Once again more accentuated effects are observed closer to the WEC, with NRMSD $> 5\%$ at 30 to 50 m away from the WEC.

Through the wave periods T_p and $T_{\mathrm{m}-10}$, we observe that the influence of the modelling approaches on the wave fields can be have a larger extent than those seen only with the H_s changes (Fig. 5.b,c). Nevertheless, for the analyzed time window (and chosen $K_t = 0.1$), these differences are < 0.1 s or $< -0.5\%$. Note that in both cases, T_p and $T_{\mathrm{m}-10}$, the largest MD and NMD (close to -5%) are observed intermediately after the WEC location and not at the location of the WEC itself as happens with H_s. It is interesting to see that the NRMSD for T_p, over 70 m away from the WEC ($> 5.5\%$), is notably larger than the values obtained for $T_{\mathrm{m}-10}$ ($\sim 1\%$). This implies that even though the mean changes in T_p, related to the modelling approaches, are small, there are constant differences in the time series of the peak period. $T_{\mathrm{m}-10}$ is obtained through integration of the wave spectrum. Thus, slight changes on the position of the energy peak do not translate as significant changes of this parameter for distances > 50 m away from the device. Closer to the position of the WEC, the NRMSD from T_p can reach values $> 15\%$ and of the order of 7% for $T_{\mathrm{m}-10}$.

B. Spectral differences

To have a wider picture of the changes introduced to the wave fields, it is necessary to analyze the effects of the WEC representation in the spectrum. In this case we analyze the omnidirectional spectrum, since the interest in centered on the energy or wave variance levels across frequencies, but the analysis could be extended to the directional spectrum. Results obtained comparing the use of a fixed $K_t = 0.1$ with respect to the time varying frequency dependent method proposed here, are presented in Fig. 6. MD, NMD and NRMSD are computed for the spectral variance levels at each discrete frequency, as done in Perignon [31] and Alday et al. [32].

Four locations are analyzed. Location A, B and C correspond to the position of the WEC and 7 m away to the NE and SE of the device (Fig. 2). Then, the fourth position is located 50 m to the East of the WEC ($x = 100$, $y = 0$). Note that this locations were selected to observe changes in the spectral characteristics where the WEC is placed and away from it.

All comparison parameters show large differences between modelling methods at A (dashed blue line), with NMD and NRMSD close to 100% across all frequencies. At the same time, these differences quickly reduce 7 m away from the center of the device at B and C. Specially between 0.1 and 0.2 Hz, MD, NMD and NRMSD are the smallest at all locations. More

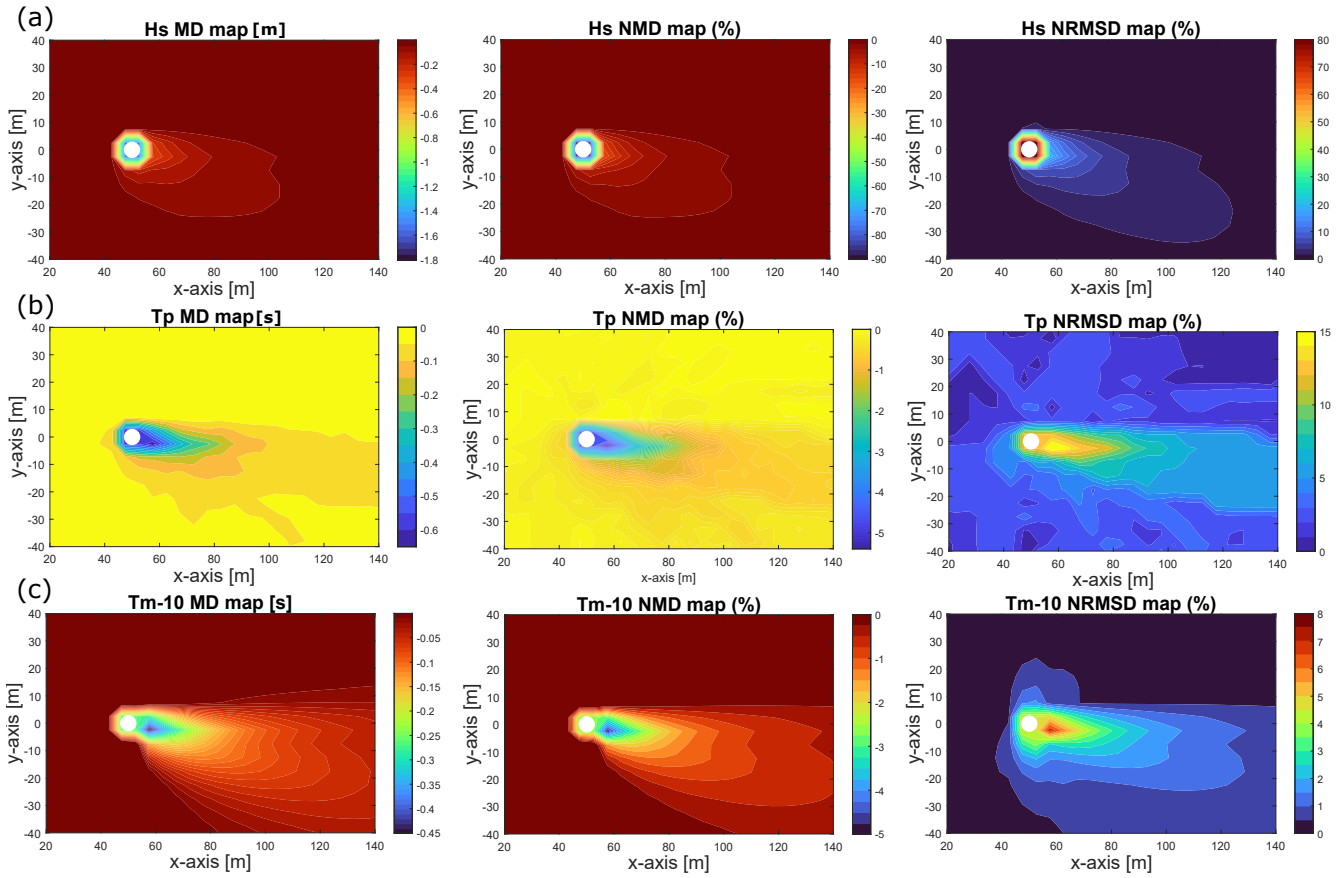

Fig. 5. Differences in (a) H_s, (b) T_p and (c) $T_{\mathrm{m}-10}$ using 2 different approaches to include WECs in SWAN. All comparisons are K_t=0.1 - $K_t(f)$(varying in time) methods. White circle indicates the position of the WEC.

interesting are the larger overall differences at frequencies between 0.05 and 0.1 Hz, and increase of NMD and NRMSD for frequencies > 0.2 Hz. Between 0.05 and 0.1 Hz is where the peaks of energy occur more frequently (not shown). It is though that the larger differences within this frequencies range is related to the poor representation of the WECs operation when a fixed K_t is employed. The same applies for the higher frequencies range. The WECs' absorbed power, after PTO adjustments, comes mostly from the range of frequencies with the largest amount of available wave energy. Thus, when using the fixed K_t approach, the amount of absorbed energy at high frequencies is largely overestimated (NMD close to -30% and NRMSD $> 30\%$ at B and C).

Although partially outside the mean wave incidence direction, the point 50 m away from the device still gives a good idea of the "attenuated" effect of the WEC. Much smaller differences are found across frequencies larger than 0.1 Hz as the wake effect becomes less dominant and the energy gradients are balanced by the incoming waves. On the other hand, NMD and NRMSD levels can still be $> 30\%$ for frequencies < 0.06 Hz.

We simulated a reduced set of idealized cases, forcing HAMS-MREL and SWAN with a JONSWAP spectrum to compare the wave fields characteristics at 25 and 50 m away from the WEC (not shown). Reconstruction of the wave spectrum using the sea surface elevation obtained in the BEM model shows that, with the proposed method, there is still an overestimation of the WEC's "shadow" effect. The overestimation of spectral variance reduction is observed mainly within the neighborhood of the peak. Nevertheless these comparisons are still preliminary and further analysis is required to properly assess accuracy of the results in SWAN, and to improve the method's tuning approach.

IV. Discussion

In the present study, a practical way to incorporate WECs in SWAN has been proposed. The main aim of this method is to improve the representation of the changes introduced on the wave fields caused by the WECs' operation. The proposed approach considers the use of a partially blocking element in SWAN with a frequency dependent and time varying transmission coefficient $K_t(f)$. This $K_t(f)$ is computed based on the estimated absorbed power per frequency, obtained using the BEM model HAMS-MREL, and the available wave power density.

To see the effects of the proposed modelling approach, the method was compared to a simpler one, considering a fixed K_t (of 0.1 in this case) for all time steps. Preliminary results showed mild changes in MD and NMD of H_s, T_p and $T_{\mathrm{m}-10}$ fields at distances over 70 m away from the WEC in the mean downwave direction. More noticeable differences are observed within the first 30 m away from the device,

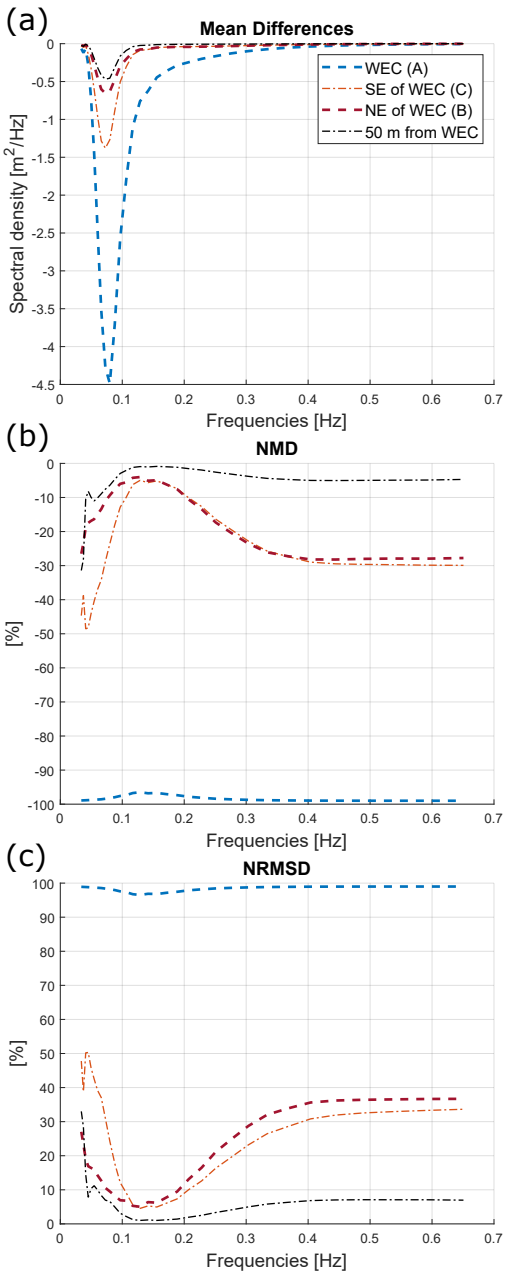

Fig. 6. Mean differences (a), NMD (b) and NRMSD (c) of spectral levels at locations A, B, C, and 50 meter away from WEC (x=100, y=0).

for example, NMD of -4.5% for H_s and close to -5% for T_p and $T_{\mathrm{m}-10}$. The NRMSD showed that changes, due to different modelling approaches, can be detected at distances over 70 m away from the WEC. It is though that this is related to the differences of the H_s, T_p and $T_{\mathrm{m}-10}$ characteristics in time.

Analysis of the wave spectrum showed that the largest differences are found at the WEC position with NMD and NRMSD close to 100%. These differences quickly decrease about 7 m away from the device, but there are still large for frequencies < 0.1 Hz and can reach NMD and NRMSD levels $> -30\%$ and up to 50% respectively. Something similar is observed for higher frequencies > 0.2 Hz. These results are of great interest since they give a clear idea of where the fixed K_t approach fails to incorporate the WECs' operation. In this case, this effect could be seen as an overestimation of the absorbed power for those frequency ranges.

The presented analysis is mainly aimed to show the implementation of the proposed method only. Further assessments and adjustments should be made to fully quantify the method's benefits regarding the WEC's effects on the wave field. Nevertheless, from the current results, we noticed that at high frequencies the sink effect of the WEC tends to be minimum. This means that the absorbed power from those frequencies is almost negligible and the reflection of the devise becomes dominant. This element should be included to improve the current method. Estimating the reflection effects could be done from the HAMS-MREL wave fields output. Similarly, radiated wave components (not considered here) could be evaluated either with HAMS-MREL or a time domain model, and thus assess how important is its inclusion. Nevertheless, it is expected that, due to its curvature, radiated waves are bound to quickly decay as they propagate away from the device. Comparisons with the sea surface amplitudes' fields from HAMS-MREL are also required to verify and validate spectral levels in the near and far fields. We consider improving the reflection considerations, perform spectral validation and testing for WEC farms in ongoing research efforts.

Although not shown, it should be mention that spatial resolution plays an important role in the results from SWAN. Additional tuning is required to adjust $K_t(f)$, when coarse resolution is employed to reduce errors in the far field wave conditions.

Acknowledgement

This work is part of the EU-SCORES project that has received funding from the European Union's Horizon 2020 research and innovation programme under grant agreement No 101036457 (https://euscores.eu)

References

[1] Y. Peña-Sanchez, D. García-Violini, M. Penalba, A. Zarketa-Astigarraga, F. Ferri, V. Nava, and J. V. Ringwood, "Control co-design for wave energy farms: Optimisation of array layout and mooring configuration in a realistic wave climate," *Renewable Energy*, vol. 227, p. 120506, 2024.

[2] D. Sarkar, E. Contal, N. Vayatis, and F. Dias, "Prediction and optimization of wave energy converter arrays using a machine learning approach," *Renewable Energy*, vol. 97, pp. 504–517, 2016.

[3] A. Babarit, "On the park effect in arrays of oscillating wave energy converters," *Renewable Energy*, vol. 58, pp. 68–78, 2013.

[4] J. Abanades, G. Flor-Blanco, G. Flor, and G. Iglesias, "Dual wave farms for energy production and coastal protection," *Ocean & Coastal Management*, vol. 160, pp. 18–29, 2018.

[5] A. R. Bento, E. Rusu, P. Martinho, and C. G. Soares, "Assessment of the changes induced by a wave energy farm in the nearshore wave conditions," *Computers & Geosciences*, vol. 71, pp. 50–61, 2014.

[6] C. E. Greenwood, D. Christie, and V. Venugopal, "The simulation of nearshore wave energy converters and their associated impacts around the outer hebrides," in *10th Eur. Wave Tidal Energy Conf.(EWTEC 2013), pp: https://doi. org/10.13140/2.1*, vol. 3963, 2013.

[7] R. Carballo and G. Iglesias, "Wave farm impact based on realistic wave-wec interaction," *Energy*, vol. 51, pp. 216–229, 2013.

[8] E. Luczko, B. Robertson, H. Bailey, C. Hiles, and B. Buckham, "Representing non-linear wave energy converters in coastal wave models," *Renewable Energy*, vol. 118, pp. 376–385, 2018.

[9] K. M. Ruehl, J. D. Roberts, A. Posner, and A. Porter, "Development of snl-swan a validated wave energy converter array modeling tool." Sandia National Lab.(SNL-NM), Albuquerque, NM (United States), Tech. Rep., 2013.

[10] M. Folley, A. Babarit, B. Child, D. Forehand, L. O'Boyle, K. Silverthorne, J. Spinneken, V. Stratigaki, and P. Troch, "A review of numerical modelling of wave energy converter arrays," in *International Conference on Offshore Mechanics and Arctic Engineering*, vol. 44946. American Society of Mechanical Engineers, 2012, pp. 535–545.

[11] C. Beels, "Optimization of the lay-out of a farm of wave energy converters in the north sea: Analysis of wave power resources, wake effects, production and cost," Ph.D. dissertation, Ghent University, 2009.

[12] V. Raghavan, E. Loukogeorgaki, N. Mantadakis, A. V. Metrikine, and G. Lavidas, "HAMS-MREL, a new open source multiple body solver for marine renewable energies: Model description, application and validation," *Renewable Energy*, vol. 237, p. 121577, 2024.

[13] N. Booij, R. C. Ris, and L. H. Holthuijsen, "A third-generation wave model for coastal regions: 1. model description and validation," *Journal of geophysical research: Oceans*, vol. 104, no. C4, pp. 7649–7666, 1999.

[14] N. Booij, L. Holthuijsen, and R. Ris, "The SWAN wave model for shallow water," in *Coastal engineering 1996*, 1996, pp. 668–676.

[15] Corpower. (2023) Corpower. [Online]. Available: https://corpowerocean.com/wave-energy-technology/

[16] J. Tan, W. Tao, A. J. Laguna, H. Polinder, Y. Xing, and S. Miedema, "A spectral-domain wave-to-wire model of wave energy converters," *Applied Ocean Research*, vol. 138, p. 103650, 2023. [Online]. Available: https://www.sciencedirect.com/science/article/pii/S0141118723001918

[17] M. Folley and T. Whittaker, "Spectral modelling of wave energy converters," *Coastal Engineering*, vol. 57, no. 10, pp. 892–897, 2010. [Online]. Available: https://www.sciencedirect.com/science/article/pii/S0378383910000700

[18] *Optimum Reactive Control and Control by Latching of a Wave-Absorbing Semisubmerged Heaving Sphere*, ser. International Conference on Offshore Mechanics and Arctic Engineering, vol. 21st International Conference on Offshore Mechanics and Arctic Engineering, Volume 4, 06 2002. [Online]. Available: https://doi.org/10.1115/OMAE2002-28172

[19] J. Tan, H. Polinder, A. J. Laguna, P. Wellens, and S. A. Miedema, "The influence of sizing of wave energy converters on the techno-economic performance," *Journal of Marine Science and Engineering*, vol. 9, no. 1, 2021. [Online]. Available: https://www.mdpi.com/2077-1312/9/1/52

[20] O. M. Mazzaretto, M. Menéndez, and H. Lobeto, "A global evaluation of the jonswap spectra suitability on coastal areas," *Ocean Engineering*, vol. 266, p. 112756, 2022. [Online]. Available: https://www.sciencedirect.com/science/article/pii/S002980182202039X

[21] M. Alday, V. Raghavan, and G. Lavidas, "Effects of wave spectrum representation on power production estimations from point absorbers," *Applied Ocean Research [in press]*, 2025.

[22] G. B. Whitham, *Linear and nonlinear waves*. John Wiley & Sons, 1974.

[23] M. W. Dingemans, *Water wave propagation over uneven bottoms (in 2 parts)*. World Scientific, 1997, vol. 13.

[24] S. Hasselmann and K. Hasselmann, "Computation and parameterizations of the nonlinear energy transfer in a gravity-wave spectrum. part I: a new method for efficient computations of the exact nonlinear transfer," *Journal of Physical Oceanography*, vol. 15, pp. 1369–1377, 1985.

[25] N. Booij, L. Holthuijsen, and M. Bénit, "A distributed collinear triad approximation in swan," in *Proceedings Of Coastal Dynamics 2009: Impacts of Human Activities on Dynamic Coastal Processes (With CD-ROM)*. World Scientific, 2009, pp. 1–10.

[26] SWAN Team *et al.*, "Swan user manual—SWAN Cycle III version 41.45 A," *Delft University of Technology: Delft, The Netherlands*, 2023.

[27] SWAN team *et al.*, "Swan, scientific and technical documentation, SWAN cycle III version 41.45," *http://www. swan. tudelft. nl, Delft University of Technology*, 2023.

[28] S. P. de Leon, J. H. Bettencourt, and N. Kjerstad, "Simulation of irregular waves in an offshore wind farm with a spectral wave model," *Continental Shelf Research*, vol. 31, no. 15, pp. 1541–1557, 2011.

[29] M. Alday and G. Lavidas, "The ECHOWAVE hindcast: A 30-years high resolution database for wave energy applications in north atlantic european waters," *Renewable Energy*, p. 121391, 2024.

[30] S. Wells, , M. Alday, J. M. Blanco, and G. Lavidas, "Assessing the impact of wec arrays on the nearshore wave climate and power production on the dutch coast," *Under Press Energy*, 2025.

[31] Y. Perignon, "Assessing accuracy in the estimation of spectral content in wave energy resource on the french atlantic test site semrev," *Renewable Energy*, vol. 114, pp. 145–153, 2017.

[32] M. Alday, F. Ardhuin, G. Dodet, and M. Accensi, "Accuracy of numerical wave model results: application to the atlantic coasts of europe," *Ocean Science*, vol. 18, no. 6, pp. 1665–1689, 2022.